Earth and Planetary Science Letters 454 (2016) 192–202

Contents lists available at ScienceDirect

Earth and Planetary Science Letters

www.elsevier.com/locate/epsl

Extreme incompatibility of helium during mantle melting: Evidence from undegassed mid-ocean ridge basalts

David W. Graham [a,*], Peter J. Michael [b], Thomas Shea [c]

[a] College of Earth, Ocean, and Atmospheric Sciences, Oregon State University, Corvallis, OR 97331, United States
[b] Department of Geosciences, The University of Tulsa, 800 South Tucker Drive, Tulsa, OK 74104, United States
[c] Department of Geology and Geophysics, University of Hawaii, Honolulu, HI 96822, United States

ARTICLE INFO

Article history:
Received 18 June 2016
Received in revised form 2 September 2016
Accepted 9 September 2016
Available online 29 September 2016
Editor: B. Marty

Keywords:
mid-ocean ridge basalt
helium
mantle melting
incompatible trace elements
ocean island hotspot

ABSTRACT

We report total helium concentrations (vesicles + glass) for a suite of thirteen ultradepleted mid-ocean ridge basalts (UD-MORBs) that were previously studied for volatile contents (CO_2, H_2O) plus major and trace elements. The selected basalts are undersaturated in CO_2 + H_2O at their depths of eruption and represent rare cases of undegassed MORBs. Sample localities from the Atlantic (2), Indian (1) and Pacific (7) Oceans collectively show excellent linear correlations ($r^2 = 0.75$–0.92) between the concentrations of helium and the highly incompatible elements C, K, Rb, Ba, Nb, Th and U. Three basalts from Gakkel Ridge in the Arctic were also studied but show anomalous behavior marked by excess lithophile trace element abundances.

In the Atlantic–Pacific–Indian suite, incompatible element concentrations vary by factors of 3–4.3, while helium concentration varies by a factor of 13. The strong correlations between the concentrations of helium and incompatible elements are explained by helium behavior as the most incompatible element during mantle melting. Partial melting of an ultradepleted mantle source, formed as a residue of earlier melt extraction, accounts for the observed concentrations. The earlier melting event involved removal of a small degree melt (~1%) at low but non-zero porosity (0.01–0.5%), leading to a small amount of melt retention that strongly leveraged the incompatible element budget of the ultradepleted mantle source. Equilibrium melting models that produce the range of trace element and helium concentrations from this source require a bulk solid/melt distribution coefficient for helium that is lower than that for other incompatible elements by about a factor of ten. Alternatively, the bulk solid/melt distribution coefficient for helium could be similar to or even larger than that for other incompatible elements, but the much larger diffusivity of helium in peridotite leads to its more effective incompatibility and efficient extraction from a larger volume of mantle during melting. In either case, partial melting leaves a mantle residue with elevated $(U + Th)/^3He$. Consequently, peridotite residues of mantle melting cannot be the source of high $^3He/^4He$ observed at ocean island hotspots such as Hawaii and Iceland.

The extreme effective incompatibility of helium entails that high $^3He/^4He$ mantle sources, isolated before 4.45 Ga based on Xe and W isotopes, have not experienced any melt extraction since they were isolated from convecting portions of the mantle.

1. Introduction

Helium isotope variations in oceanic basalts have been of central importance to the field of chemical geodynamics. High $^3He/^4He$ ratios observed at localities such as Hawaii and Iceland are a key line of evidence for the existence of mantle plumes (Kurz et al., 1982). The high $^3He/^4He$ ratios (up to 50 R_A, where R_A is the ratio in air) compared to those in mid-ocean ridge basalts (MORBs, which typically have $^3He/^4He$ = 6–10 R_A) require a mantle source region with a lower time-integrated $(U + Th)/^3He$ ratio. These hotspot or plume source regions must have remained effectively isolated over Earth's history, probably because they are located deeper and are less degassed than the upper mantle source region for MORBs (e.g., Porcelli and Elliott, 2008). Ne–Ar–Xe isotopic systematics in oceanic basalts are fully consistent with this inferred mantle structure (e.g., Marty, 2012; Mukhopadhyay, 2012; Moreira, 2013).

* Corresponding author.
E-mail addresses: dgraham@coas.oregonstate.edu (D.W. Graham), pjm@utulsa.edu (P.J. Michael), tshea@hawaii.edu (T. Shea).

http://dx.doi.org/10.1016/j.epsl.2016.09.016
0012-821X/

Other geochemical evidence complicates this simple and coherent picture from the noble gases. High $^3He/^4He$ ratios at ocean island hotspots are often associated with "isotopically depleted" compositions of Nd, Sr and Pb that approach those seen in MORBs (Class and Goldstein, 2005). This complex behavior might arise through melt extraction and trace element depletion that affected the whole mantle. According to this model, deep island sources today would have retained a higher $^3He/(U+Th)$ ratio during ancient melting events when that mantle ascended beneath a mid-ocean ridge. The higher $^3He/(U+Th)$ might result either from a small amount of melt retention in the residue (Davies, 2010), or through elemental fractionation during the partial melting process. For example, Albarède (1998) suggested that recycled, depleted oceanic lithosphere in the mantle source region of ocean islands could lead to elevated $^3He/^4He$ because He behaves as a less incompatible element compared to U and Th during melt depletion events.

The behavior of U and Th during partial melting of spinel peridotite is dominated by the presence of clinopyroxene, which has a range of experimentally determined mineral/melt partition coefficients (k) that depend on pressure, temperature, mineral composition and oxygen fugacity. Values of k_U and k_{Th} in clinopyroxene range from 3.4×10^{-3} to 1.8×10^{-2} and 8×10^{-3} to 3.6×10^{-2}, respectively (LaTourrette and Burnett, 1992; Beattie, 1993a; Blundy and Wood, 2003; McDade et al., 2003). Values of k_U and k_{Th} in garnet are approximately 9×10^{-3} to 1.8×10^{-2} and 1.5×10^{-3} to 3.3×10^{-3} (LaTourrette et al., 1993; Beattie, 1993b).

There is also a long history of experimental determinations of helium partition coefficients relevant to mantle melting (Hiyagon and Ozima, 1986; Brooker et al., 2003; Parman et al., 2005; Heber et al., 2007; Jackson et al., 2013). These measurements have many complications and have sometimes provided conflicting interpretations. Numerical values for noble gas partitioning are sometimes argued to be maxima even when factors such as the presence of bubbles have been reduced or eliminated. While earlier estimates (e.g., Parman et al., 2005) were notably above 10^{-3}, recent determinations indicate a median helium partition coefficient of $\sim 2 \times 10^{-4}$ between peridotitic phases (olivine, clinopyroxene, orthopyroxene) and basaltic melt at mantle conditions (Heber et al., 2007; Jackson et al., 2013). Marty and Lussiez (1993) and Kurz (1993) used paired analyses of coexisting olivine and basalt glass of Atlantic MORBs to estimate the olivine–melt partition coefficient for helium and obtained values of 6 to 8×10^{-3}. These natural values represent upper limits because the olivines contained melt inclusions and the basalt glasses were partially degassed. The recent studies of Heber et al. (2007) and Jackson et al. (2013) suggest He is similar to or more incompatible than U and Th during early partial melting (e.g., of lherzolite), but perhaps He is more compatible at more advanced stages of melting (e.g., of harzburgite or dunite). This latter possibility would imply that depleted residues of ancient mantle melting might have high $^3He/(U+Th)$ and could ultimately be the source for high $^3He/^4He$ ratios at ocean island hotspots.

In principle, the bulk solid/melt distribution coefficient (K_{He}) for helium during mantle melting can also be estimated from concentration measurements in naturally occurring basalts. The extent of melting needs to be known and adjustment must be made for crystal fractionation; the choice of a melting model also influences the estimate and leads to some ambiguities. With highly incompatible elements that can only be fractionated from each other at very low extents of partial melting, a common approach is to estimate the source elemental ratios for a suite of variably depleted lavas and then determine the relative incompatibility of several elements. For volatile elements such as helium this is complicated by the fact that virtually all submarine basalts are oversaturated in their major volatiles ($CO_2 + H_2O$) and consequently they will have lost an unknown amount of helium by degassing. Although degassing corrections can be made in favorable cases, for example using the $^4He/^{40}Ar^*$ ratio, estimates of parental magma helium concentrations and source ratios of helium to other trace elements are uncertain. In this study we use a suite of mid-ocean ridge basalts that are undersaturated in major volatiles at their eruption depth (Michael and Graham, 2015). This sample suite allows a basic test of the behavior of helium during partial melting relative to other incompatible elements (U, Th, K, Rb, Nb, Ba and C). Our results indicate that helium effectively behaves as the most incompatible element during upper mantle melting. Two important conclusions stemming from this result are that peridotitic melting residues are not the origin of high $^3He/^4He$ ratios at ocean island hotspots, and that retention of helium in convecting mantle over Earth history is extremely unlikely, lending further support for the isolation of relatively primitive material deep in the planet.

2. Material and methods

The samples for this study are a suite of undegassed mid-ocean ridge basalt glasses previously studied for major volatiles ($CO_2 + H_2O$), and major and trace elements (Michael and Graham, 2015). Major elements were determined by electron microprobe analysis or published values have been used. Trace elements were determined by laser ablation ICP-MS (inductively coupled plasma mass spectrometry). Vesicle He contents and $^3He/^4He$ were measured by mass spectrometry and CO_2 contents were determined by capacitance manometry, following *in vacuo* crushing of approximately 250–400 mg of glass chips (typically one to four mm-size pieces). All samples had <3 ppm vesicle CO_2 as expected for their undersaturated nature and the general absence of vesicles. Helium amounts released by crushing were also low, between 1.6×10^{-8} and 9.2×10^{-7} ccSTP/g, and comprised 1–8% of the total helium released by melting glass chips (see below). Dissolved CO_2 and H_2O were determined by FTIR spectroscopy. Detailed descriptions of the sample locations are reported in Michael and Graham (2015). The lavas are all relatively primitive and have Mg# between 61 and 71. Trace element contents are very low, in keeping with the primitive and depleted nature of these magmas; [Nb] varies from 0.2 to 1.3 ppm, [K] from 90 to 625 ppm, and [La] from 0.9 to 2 ppm. Sample collection depths are close to their eruption depths based on knowledge of the dredge locations. All samples are volatile undersaturated based on comparison to the computed saturation concentrations using VolatileCalc (Newman and Lowenstern, 2002).

In this study, millimeter size glass chips ranging in weight from ~60 to ~100 mg were loaded into a stainless steel carousel that allowed samples to be sequentially dropped into a high temperature resistively-heated vacuum furnace. Glasses were melted at 1450 °C, the released gases were processed through a series of SAES getters to remove active gases, and the noble gases were cryo-sorbed onto activated charcoal at 10 K. Helium was selectively released from the cryogenic trap at 45 K and admitted to the mass spectrometer. Analyses were carried out as described previously in Graham et al. (2014). Furnace hot blanks, routinely analyzed before and after each sample, averaged $1.2 \pm 0.3 \times 10^{-10}$ ccSTP ^4He and were always <0.1% of the sample size.

3. Results

Analytical results are reported in the Supplementary Table S1.

3.1. Incompatible trace element variations

Trace element concentrations are very low. While the moderately incompatible elements (La through Lu) overlap with canonical values for normal mid-ocean ridge basalts (N-MORB), the highly incompatible elements (Cs, Rb, Ba, Th, U, Nb, Ta, K) are

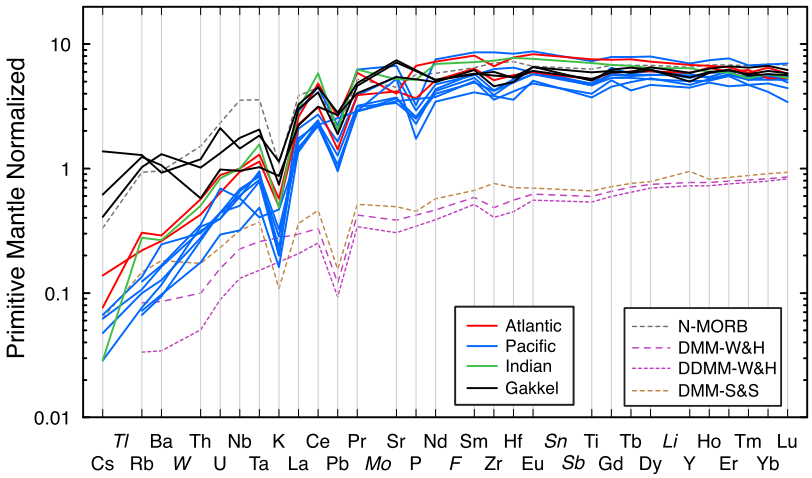

Fig. 1. Primitive mantle-normalized spider diagram for undegassed mid-ocean ridge basalt glasses of this study. Trace element data are reported in Supplementary Table S1, and normalizing values are from Sun and McDonough (1989). Italicized elements have not been analyzed. The undegassed MORBs shown here are uncorrected for the small amounts of crystal fractionation that occurred in this suite; assuming a parental magma with Mg# = 68 the extent of crystallization ranges from ~3–14% for Atlantic–Pacific–Indian samples (see calculated adjustment factors reported in Table S1). Any corrections for crystal fractionation shift the most incompatible elements on the left-hand side of the diagram to even lower and more depleted values. Also shown for reference are patterns for N-MORB (Sun and McDonough, 1989), depleted MORB mantle from Workman and Hart (2005) and Salters and Stracke (2004) (DMM-W&H and DMM-S&S, respectively) plus ultradepleted MORB mantle (DDMM) from Workman and Hart (2005).

lower than canonical N-MORB values by as much as a factor of ten (Fig. 1). The samples of undegassed lava studied here are classified as ultradepleted MORBs (UD-MORBs) because they have the lowest trace element concentrations yet measured in MORB glasses (Michael and Graham, 2015). We use the term undegassed MORBs to refer to a subset of the UD-MORBs studied by Michael and Graham (2015). These undegassed MORBs are volatile undersaturated at their depth of eruption, and so do not include trace element or gas-rich samples such as popping rocks. The Atlantic and Indian undegassed samples as a group have somewhat higher trace element contents compared to the Pacific group. In contrast, the three Gakkel Ridge undegassed MORBs are not as depleted, with Rb and Ba contents similar to the N-MORB composition of Sun and McDonough (1989), and show a less marked decrease and more variable behavior with increasing element incompatibility in the spider diagram (Fig. 1).

Typical MORBs (depleted, transitional and enriched types) display negative covariations of the highly incompatible elements when normalized to La and plotted versus Ce/La ratio (Fig. 2). It is common practice to use ratios such as La/Ce or La/Sm to investigate differences in degree of LREE enrichment; using the Ce/La ratio accentuates small differences in degrees of LREE depletion. The negative covariations displayed by Rb, Nb, Ba and Th for MORBs (including popping rocks and olivine hosted melt inclusions) show trends that intersect the undegassed MORBs of this study at values of Ce/La near 3.5. However, the undegassed MORBs display flat trends on these diagrams that extend to Ce/La ratios of 5. These MORBs are therefore unusual, and in general they are not a mixing end-member for global MORB geochemical variations.

3.2. Helium – carbon dioxide relations

Total $CO_2/^3He$ ratios in undegassed MORBs range from 3.6×10^8 to 2.8×10^9 (Fig. 3). Nearly the full range of $CO_2/^3He$ is observed in the Pacific MORBs alone, where the ratio is mostly controlled by variations in ^3He concentration. In the Pacific suite, CO_2 ranges by more than a factor of 1.5 while the ^3He concentration varies by a factor of ten. The range of $CO_2/^3He$ ratios in the current study is within the typical MORB range of $0.2–3 \times 10^9$ (Marty and Jambon, 1987; Marty and Zimmerman, 1999; Graham et al., 2014).

3.3. Helium – trace element relations

Helium concentrations are well correlated with the concentrations of the highly incompatible trace elements (Fig. 4). Excluding the Gakkel Ridge basalts, linear correlation coefficients vary between 0.76 and 0.92 for K, Rb, Ba, Nb, Th and U. The x–y systematics are consistent with helium behaving as the most incompatible element based on the observed y-axis intercepts (e.g., Allègre et al., 1977) for the correlations of helium with each of the above elements. Additionally, all trace element concentrations show a narrower range of relative variations compared to helium. For the Atlantic, Pacific and Indian undegassed MORB glasses the factors of variation are Rb (4.3), K (3.5) and Th, U, Nb and Ba (3.0–3.2), while the helium concentration ranges by a factor of 13. When Gakkel Ridge samples are included the factors of variation are Rb (19.3), Ba (12.7), Th (10.0), U (7.7), K (7.0) and Nb (6.1), while for helium the concentration ranges by a factor of 19.6. The three undegassed Gakkel Ridge basalts clearly show less depletion in the highly incompatible elements when compared to the Atlantic, Pacific and Indian lavas. Unusual behavior for elements such as Ba, Rb and U in Arctic MORBs was noted previously (Michael et al., 2003; Goldstein et al., 2008) and attributed to recent stirring of subcontinental mantle into the asthenosphere (Goldstein et al., 2008).

4. Discussion

4.1. Partial melting and origin of the undegassed and ultra-depleted MORB suite

Most basalts from the global mid-ocean ridge system show negative covariations for Rb, Nb, Ba and Th with Ce/La that intersect the undegassed MORBs at values of Ce/La near 3.5, while the undegassed MORBs show relatively flat trends on Fig. 2 that extend to higher Ce/La ratio. The process responsible for the overall negative trend for global MORBs in Fig. 2 therefore cannot explain the ultra-depleted MORBs. The UD-MORB mantle source is special, and it may have been affected by processes that disturbed incompatible element concentrations and their ratios. Compared to other MORBs, the highly incompatible elements such as Rb, Nb, Th and Ba show depletion relative to slightly less incompatible elements such as La during petrogenesis of the ultra-depleted MORBs (Michael and Graham, 2015). This indicates that the volatile/trace

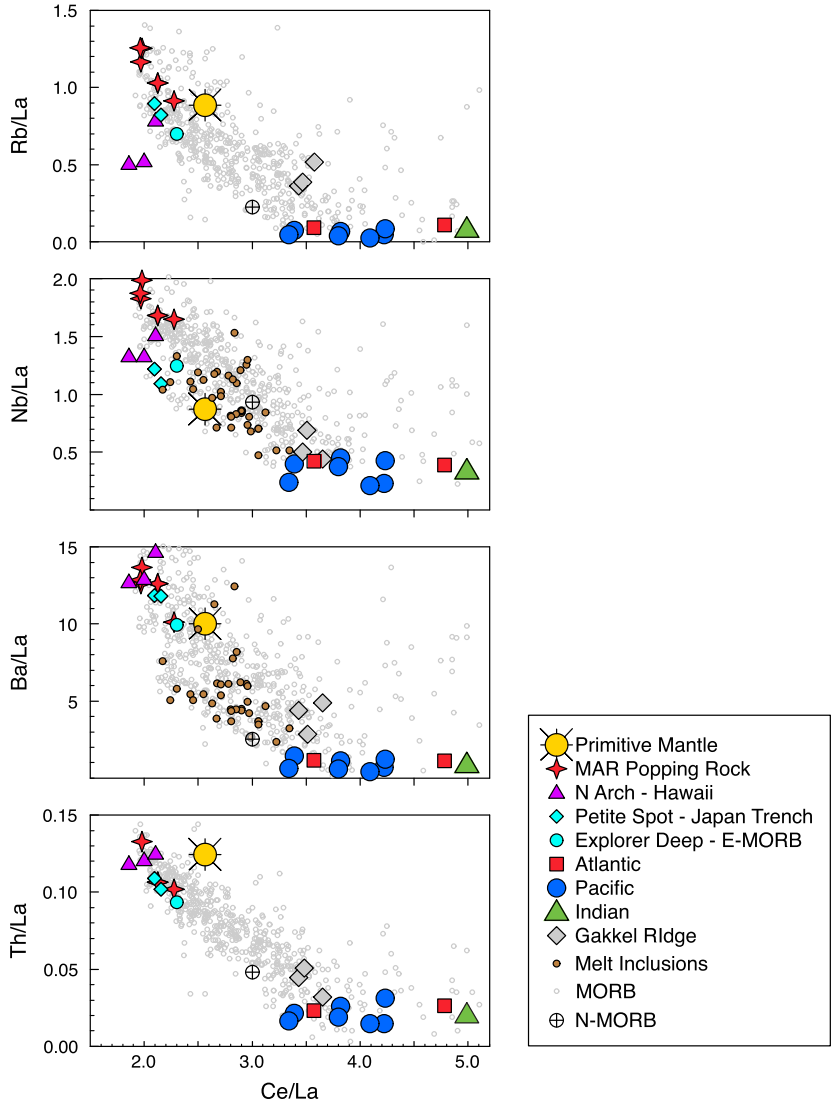

Fig. 2. Multi-element plots of highly incompatible lithophile elements (Th, Nb, Ba, Rb relative to La) vs. Ce/La ratio. MORBs, in gray, are from Kelley et al. (2013). MAR popping rock from Bougault et al. (1988) and Cartigny et al. (2008); North Arch Hawaii basalts from Dixon et al. (1997); olivine-hosted melt inclusions from Wanless and Shaw (2012), Helo et al. (2011) and Hartley et al. (2014); petite spot volcanoes from Hirano et al. (2006); Explorer Deep from Michael and Graham (2015).

element ratios in these samples should be interpreted with care. Michael and Graham (2015) noted that neither CO_2/Ba nor CO_2/Nb vary significantly with ratios such as Ce/La or La/Nb. The negative trend for global MORBs in Fig. 2 might be accounted for by mixing. This mixing would involve enriched low degree melts or E-MORB source mantle as one component. N-MORB source mantle or an N-MORB mantle residue that experienced prior removal of a small degree partial melt (Michael and Graham, 2015) would be the other component. It is noteworthy in this context that the most depleted UD-MORB source, having high Ce/La, cannot be a mixing end-member for the global MORB array because it is too depleted in incompatible trace elements (Fig. 2). In addition, the flat trend for the undegassed MORBs on Fig. 2 suggests that they may be related as a group to different degrees of source depletion, or partial melting and mixing of two highly depleted end-members.

It is evident from ratios like La/Nb and Ce/La that the UD-MORB mantle source underwent a prior melt-loss event. This is also evident from the CO_2/H_2O ratio, which is anomalously low (mass ratio of 0.07–0.23) compared to typical depleted MORB values of 0.55 ± 0.2 (Hirschmann and Dasgupta, 2009). The low CO_2/H_2O of the undegassed MORBs also corresponds to lower chondrite-normalized La/Sm (0.25–0.43) than depleted mantle (~0.5), so they lie below the trend for the upper mantle defined by Hirschmann and Dasgupta (2009). This feature appears to extend to other volatile element ratios such as He/CO_2 because the most depleted of the undegassed MORBs (from the Pacific) trend to lower He/CO_2 ratios (Fig. 3).

Our results for the undegassed MORB suite suggest that He behaves more incompatibly than the other trace elements, and a full explanation needs to account for the effects of both the early melt-loss event from the MORB source and the subsequent generation of UD-MORB liquids. In the sections below we explore two different partial melting models that help to explain the extremely incompatible behavior of helium compared to other highly incompatible lithophile elements. The first model (Model A) produces the ultra-depleted mantle source via a small amount of melt removal from a normal MORB source. During both this earlier stage of melting and the second stage that produces the undegassed MORB liquids, helium is fractionated from other elements because it is the most incompatible element, consistent with recent experimental data for mineral–melt partition coefficients. The second model (Model B) is a disequilibrium melting model, in which elemental concentrations in the melt are strongly affected by diffusion rates in the

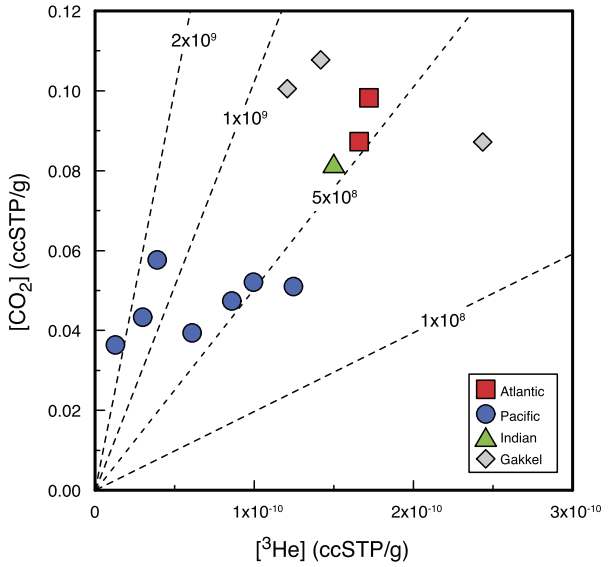

Fig. 3. Total $[CO_2]$ (vesicle + glass) vs. total $[^3He]$ for undegassed MORBs. Simple regression analysis of all data gives $[CO_2] = 3.0 \times 10^8 [^3He] + 0.036$, $r^2 = 0.57$; excluding the Gakkel Ridge basalts, $[CO_2] = 3.2 \times 10^8 [^3He] + 0.029$, $r^2 = 0.74$.

solid mantle. Model B also requires some prior melt removal from a peridotitic source, and it allows for helium diffusivity in the mantle that is much higher than for Th and U by utilizing diffusion rate estimates from experimental data. In the model B cases investigated, we also make the conservative assumption that helium is as compatible, or even more compatible than Th and U during both stages of melting. This demonstrates that knowing the precise values of He, U and Th solid/melt partitioning during melting is less critical than knowing their relative mobilities for this type of model explanation. While we recognize that more complex melting models may eventually be needed to account for all aspects of the UD-MORB geochemical variations, we focus our attention in this work on model effects that bear on the relationships between He and the highly incompatibly elements, and we primarily utilize Th as an example element because of its involvement in radiogenic ^4He production and the fact that it is measured more precisely than U at these low concentration levels.

4.1.1. Model A: extreme helium incompatibility during solid/melt partitioning

The first model we present involves production of the ultra-depleted mantle source through an early melt-loss event, followed by a second stage of aggregated fractional melting to produce the suite of UD-MORBs. Two criteria in this model help to produce the large fractionation between helium and incompatible elements during melting and still achieve the measured concentration level in the ultra-depleted MORBs. These are 1) a small degree of melt retention in the initially depleted source, and 2) a bulk distribution coefficient for helium (K_{He}) in each stage of melting that is lower than that for the other incompatible elements.

Results of simple forward models are described in the Supplementary Information. The most salient results are illustrated here using a diagram of He/Th vs. [He] (Fig. 5). Various amounts of batch melt were removed; Fig. 5 illustrates the example of 1% melt removed in stage 1. The amount of retained (trapped) melt during stage 1 varies; in the example shown in Fig. 5 the range is from 0.02% to 0.5%. A small amount of trapped melt during this earlier melt extraction is required in order to eventually match the observed range of He concentrations, otherwise the UD-MORB source becomes too depleted in helium and other highly incompatible elements. The model produces an ultra-depleted mantle source that is subsequently melted in the second stage of melting to between 10 and 20%, producing ultra-depleted MORBs via aggregated fractional melting. There are model tradeoffs between the amount of melting in the first-stage, the percentage of melt retained (residual porosity), and the degree of melting in the second stage. Only some combinations lead to the observed range of He/Th in the undegassed MORB suite and simultaneously produce melt compositions that have sufficiently high He concentrations (Fig. 5). While there is no unique solution with such a simple forward modeling approach, the low He/Th ratios observed in the undegassed MORBs are only produced when $K_{He} < K_{Th}$ using this simple, two-step melting model. This is fully consistent with the experimental observations of Heber et al. (2007) and Jackson et al. (2013).

In principle, the timing of earlier melt-loss events may be addressed from isotopic variations in the UD-MORBs, although more than one event may have occurred and a young event may not be resolvable isotopically. A complete set of isotopic data is not available for every sample, but many of the samples have been analyzed for Sr–Nd–Pb and all have been analyzed for He isotopes (previous work and this study; see supplementary information). The two Atlantic lavas span the full range of $^{87}Sr/^{86}Sr$ in the undegassed MORB suite, from 0.70213 to 0.70287. These samples have corresponding ε_{Nd} of 11.6 and 8.9, respectively. In contrast, the highly depleted Pacific samples ENV7123-3-5 and ALV2384-001 have intermediate $^{87}Sr/^{86}Sr$ of 0.70236 and 0.70255. $\varepsilon_{Nd} = 12.7$ for ALV2384-001 from the Siqueiros Transform, but a Nd isotope analysis is not yet available for the most trace element-depleted sample ENV7123-3-5. These ranges of values indicate that while the UD-MORBs are usually the most isotopically depleted samples locally, and they have a component of ancient melt depletion that is a well-known characteristic of the upper mantle (e.g., Gast, 1968), they do not show systematic isotope-trace element variations indicating a single melt-loss event. Moreover, the undegassed MORBs of this study show a range of $^3He/^4He$ from 7.45 to 8.82 R_A, but there is no systematic variation with trace element ratios or Sr–Nd–Pb isotopic variations. Extensive study of mid-ocean ridge basalts has revealed a general pattern of $^3He/^4He$ ratios near 9 R_A, or even higher, in the locally most depleted lavas, and this feature appears to be widespread and perhaps global in extent. Examples include the Juan de Fuca Ridge (8.8 R_A, Lupton et al., 1993), equatorial and northern portions of the South Atlantic (8.8–9.3 R_A, Graham et al., 1992; Tucker et al., 2012; Stroncik and Niedermann, 2016), the Garrett Transform region of the East Pacific Rise (9.7 R_A, Kurz et al., 2005), the Southwest Indian Ridge (9.8 R_A, Gautheron et al., 2015), the Pacific/Antarctic Ridge (Hamelin et al., 2011) and the Southeast Indian Ridge (9.7–10.2 R_A, Graham et al., 2001, 2014). The undegassed MORBs of the current study do not extend to these higher MORB values, with the exception of the Equatorial Atlantic sample RC2806 D1 (8.8 R_A). If the elevated $^3He/^4He$ observed previously in highly depleted MORB glasses was caused by an ancient melt depletion event in the upper mantle, as suggested by Stroncik and Niedermann (2016), then the general absence of such elevated values in the undegassed MORB suite implies that ancient melting may not have produced their unusual trace element characteristics. This points to a possible "young" melt loss event in their genesis, perhaps associated with melt migration and transport beneath the modern spreading ocean ridge system. It is noteworthy in this regard that recent modeling by Keller et al. (in press) suggests that a significant amount of deep, volatile-rich melt may escape eruption at the ridge axis and become trapped along the lithosphere–asthenosphere boundary.

Indeed, the UD-MORB lavas are typically not recovered from ridge segment centers, and often come from somewhat unusual settings including near transform faults or along intra-transform relay zones, or associated with the periphery of mantle hotspots. An 'extra' component of lateral flow and possible lateral escape

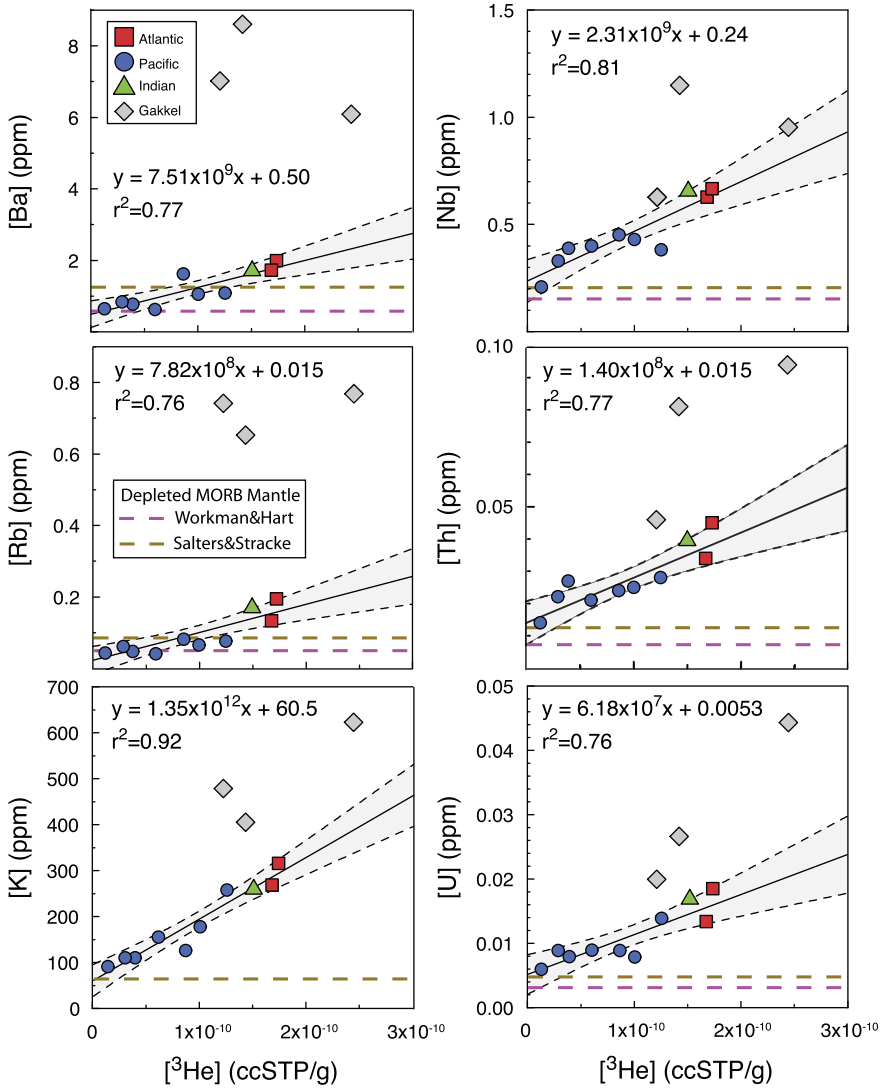

Fig. 4. Incompatible lithophile element correlations with ^{3}He. All lithophile elements are in ppm and ^{3}He is in ccSTP/g. Linear regression equations and correlation coefficients reported on each panel exclude the three anomalous samples from Gakkel Ridge. The shaded regions delineate 95% confidence for each regression. Horizontal dash lines delineate the concentrations of lithophile elements in the solid, depleted MORB mantle estimated by Workman and Hart (2005) and Salters and Stracke (2004).

of small-degree melts during upwelling of sub-ridge mantle can account for many of the geochemical variations along spreading centers near transform faults (Gregg et al., 2009). The lateral escape of small degree melts from upwelling mantle regions beneath spreading ridges has also been suggested as a cause for metasomatism of oceanic lithosphere (Pilet et al., 2011; Keller et al., in press).

4.1.2. Model B: diffusion controlled differences in effective incompatibility

The second model we explore also involves formation of the ultra-depleted mantle source through a prior melt-loss event as required by the trace element patterns (Fig. 1). This model differs from Model A because the bulk solid/melt distribution coefficient for He (K_{He}) during melting is assumed to be equal to or larger than the solid/melt distribution coefficient for other highly incompatible elements. However, in this model we further consider the strong contrast in element mobility in the solid mantle during the melting process. We chose to explore this model using conservative assumptions about partition coefficients to demonstrate that the precise choice of numerical values for solid/melt partitioning may be of lesser importance than diffusion rates, particularly when comparing elements that differ in their mobility by orders of magnitude. Models of this type have been developed previously (e.g., Qin, 1992; Van Orman et al., 2002) but the diffusion rate contrasts that were originally studied were far less extreme than what we consider here in comparing large-ion lithophile elements with the noble gases. We adapted the Qin (1992) model formalism to study fractionation of He from other highly incompatible elements, utilizing recent estimates of diffusion rates and model parameters described below and in the Supplementary Information.

Diffusion rates for helium in olivine vary between $\sim 10^{-13}$ and 4×10^{-11} m^2/s in the temperature range 1300–1500 °C (Fig. S4). The nature of helium diffusion in mantle minerals was briefly reviewed by Hart et al. (2008), and seems to be faster in both clinopyroxene and garnet at mantle temperatures. Th is expected to diffuse slowly. For instance, in diopside Th diffuses at rates intermediate to Al and Si, at about 10^{-20}–10^{-21} m^2 s^{-1} at mantle temperatures (Cherniak and Dimanov, 2010). To be conservative, we simply assume that the upper limit for Th diffusivity is that of the faster divalent cations such as Fe–Mg (Fig. S4). We note that slower diffusivities for Th would only enhance He–Th decoupling during the effects of disequilibrium melting.

Because the disequilibrium melting model B developed herein investigates scenarios in which He is as compatible (or more com-

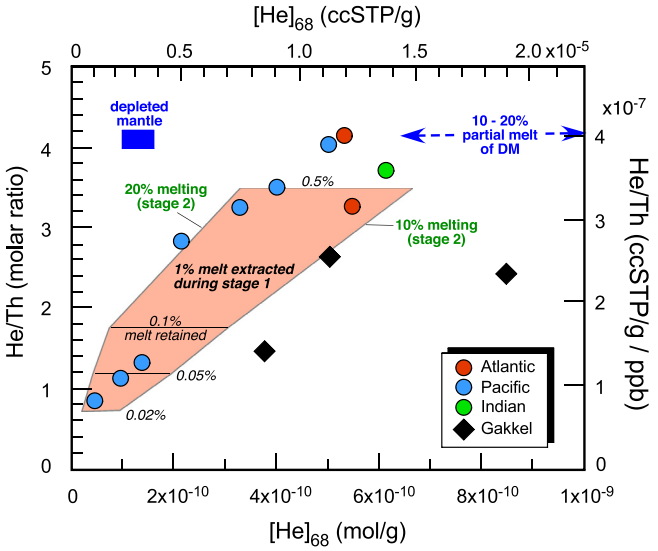

Fig. 5. Model A results using aggregated fractional melting in which the solid/melt incompatibility for helium is larger than for U and Th. Data points show the undegassed MORB samples of this study. $[He]_{68}$ in undegassed MORBs is the helium concentration in each sample corrected for small amounts of fractional crystallization as described by Michael and Graham (2015) (adjustment factors are reported in Table S1). The initial unmelted MORB source shown by the blue box was selected to have depleted mantle characteristics of Porcelli and Elliott (2008). Ultradepleted source formation involves a first stage of partial melting and melt loss of 0.1–2%. The example shown here is for 1% melting with a range of residual porosity between 0.02–0.5%. This hybrid, UD-MORB source has lower He/Th ratios than the original depleted mantle source because of the small amount of prior melt loss, and its finite residual porosity largely dictates its helium concentration. This source is remelted in a later event, and the fractional melts are aggregated from between 10–20% melting, producing arrays of melts that lie in the orange field. For the example shown here the bulk distribution coefficients are $K_{He} = 1.8 \times 10^{-4}$ and $K_{Th} = 2.3 \times 10^{-3}$. (For interpretation of the references to color in this figure legend, the reader is referred to the web version of this article.)

patible) as Th ($k_{He} \geq k_{Th}$), we implemented two sets of values: a first set of models were run with $k_{He} = k_{Th} = 10^{-3}$, and another with $k_{He} = 10^{-3}$ and $k_{Th} = 10^{-4}$. Parameter choices for melting rate, grain size, and critical porosity used in the Qin (1992) model are described in the Supplementary Information. The Qin (1992) parameter space is largely captured by the dimensionless non-equilibrium number Ne $\# = vR_0^2/D$, where v is melting rate, R_0 is grain size and D is diffusivity, and it describes characteristic domains on a diagram of element diffusivity vs. melting rate (Fig. S5).

A single stage melt extraction in Model B is incapable of generating the He concentrations and range of He/incompatible element ratios observed in the undegassed MORBs (see Fig. S6 for details). A two-stage melting model can produce the observed range of He concentrations and He/Th ratio. Two-stage melting results using the Model B formalism are shown in Fig. 6 for the case where $k_{He} \geq k_{Th}$ (the case for $k_{He} \leq k_{Th}$ is also reported in Fig. S7). A small residual porosity (typically 0.1–1% trapped melt) is again required in order to maintain a sufficiently high [He] in the depleted source so that melting in the second stage produces magma with the He/Th and He concentrations observed in the undegassed MORBs. As expected, larger degrees of melting of this depleted source produce somewhat lower He/Th for any given porosity, and significantly lower [He], similar to what was observed in Model A.

A number of studies have discussed how aspects of melt transport can generate disequilibrium effects during melt generation beneath mid-ocean ridges (e.g., Navon and Stolper, 1987; Spiegelman and Kenyon, 1992; Hart, 1993). A first-order conclusion is that as melts form and traverse regions of the mantle where they are not in equilibrium, the extent to which they interact with ambient mantle depends on the spacing of melt channels and of mantle lithologic heterogeneities and how they are distributed (e.g., as veins, pods, etc.; Spiegelman and Kenyon, 1992). In addition, both diffusive and reaction fronts may be developed in the solid, and these will differ for various elements depending on their solid/melt compatibility and diffusion rate in the solid (Navon and Stolper, 1987). Based on our forward modeling that considers such diffusive effects, by using realistic parameter choices and conservative choices for solid/melt distribution coefficients, we find that a two-stage melting model adequately describes the observed variations in helium/incompatible element ratios and in He concentrations. Effectively this means that the volume of mantle being sampled for He during melting may vary with the extent of melting, and may greatly exceed the volume sampled by other elements. This occurs because He is at least 2–4 orders of magnitude more mobile in the solid mantle than large-ion lithophile trace elements.

It is notable that the three most depleted undegassed MORBs (from the Pacific) trend to lower He/CO_2 ratios (Fig. 3). This observation is consistent with Model A if carbon has a distribution coefficient during melting that is similar to that for Th. It may also be consistent with model B if the diffusivity of helium is significantly faster than that for carbon. Very little experimental data are available for carbon diffusivity. In olivine, carbon appears to be dissolved as C^{4+} (Shcheka et al., 2006). Its diffusion coefficient in olivine at 1100 °C was determined to be $\sim 1 \times 10^{-15}$ cm^2/s (Shilobreeva et al., 2000), which is not much slower than the value for helium at this temperature ($\sim 1.5 \times 10^{-15}$ cm^2/s). However, carbon mobility in the mantle depends strongly on the phase in which it is located. At depths shallower than ~250 km, carbon could be highly mobile if it is present as a melt such as carbonatite (Dasgupta and Hirschmann, 2006). At greater depths, carbon in the asthenosphere is probably hosted as graphite or diamond (Stagno et al., 2013). The solubility of carbon in silicates is very low (Shcheka et al., 2006) and its diffusion through silicate grains is unlikely to be an appreciable mode of transport. Grain boundary diffusion has been proposed to be a key process for transport of carbon (e.g., Hayden and Watson, 2008) but quantifying it rests on several assumptions, including knowing the grain size distribution in the mantle which itself is a controversial topic. Burnard et al. (2015) performed experiments showing that grain boundaries can also be important sites for noble gas storage, but they showed that grain sizes and temperatures relevant to the mantle lead to similar diffusivities for grain boundary helium vs. lattice-hosted helium.

There is also potential for isotopic fractionation of ^3He from ^4He by diffusive processes during melting (Burnard, 2004). Although it is not possible to adequately address this issue with a small and global data set such as the undegassed MORBs, we note that there is no systematic variation of $^3He/^4He$ with He concentration or with ratios such as He/Th in this sample suite. The absence of such a covariation might mean that diffusive fractionation during melting as described in Model B has not significantly affected the $^3He/^4He$ ratio for the undegassed MORBs. Trull and Kurz (1993) also concluded that significant isotopic fractionation of residual mantle helium was unlikely given that their measured diffusivities for ^3He were only marginally higher than for ^4He ($4 \pm 4\%$ faster in pyroxene and $9 \pm 4\%$ in olivine).

In summary, the observation that helium is the most incompatible element during melting is consistent with the best experimental evidence on helium partition coefficients (Heber et al., 2007; Jackson et al., 2013). Faster diffusivity of helium in the mantle during melting is not required to explain the undegassed MORB results, but it also cannot be ruled out as a factor. In the unlikely situation that relative values of partition coefficients for helium vs. highly incompatible elements were reversed from the best experimental estimates (i.e., with helium being more compatible during

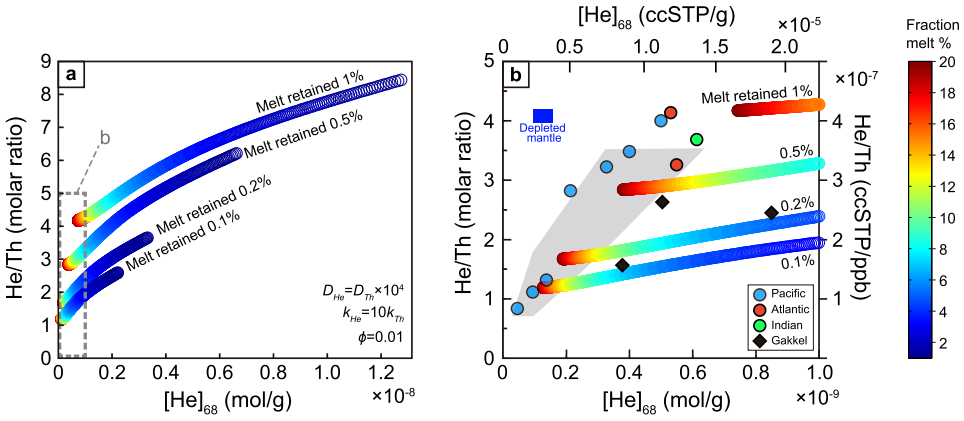

Fig. 6. Two-stage melting model results for Model B, in which the effective solid/melt partitioning is influenced by mantle diffusion rate. In the cases shown here the non-equilibrium number Ne# = 5.1×10^{-5} for He and 0.51 for Th. (a) Color-coded curves show variations in He/Th vs. [He] as a function of melt produced (0–20%) using four different amounts of melt retained after stage 1 melting (0.1 to 1%). All models assume the same diffusivity difference between He and Th ($D_{He} = 10^4 D_{Th}$), a critical porosity of 1%, and a He solid/melt partition coefficient that is 10 times larger than the value for Th. (b) Enlarged region of (a) compares the model results to values observed for the undegassed MORBs, where $[He]_{68}$ in is the helium concentration in each sample corrected for small amounts of fractional crystallization. The shaded region shows the range of model A results (Fig. 5) for comparison. In general the topology of Model A and Model B results is similar.

melting), the kinetic effects would be required and could lead to results similar to what is observed in the undegassed MORBs.

4.2. Helium behavior in the Earth and mantle structure

The presence of elevated $^3He/^4He$ in mantle-derived rocks has often been regarded as a conundrum in mantle geochemistry. A volatile-rich primordial reservoir is not expected to survive the high temperatures associated with planetary accretion that led to differentiation, melting and degassing (e.g., Anderson, 1998), and so it has been suggested that much of the mantle may be depleted, degassed and refractory. One suggestion is that helium with high $^3He/^4He$ ratios (along with Ne having a solar signature) diffused into residual refractory rocks, such as dunite, from enriched mantle rocks early in Earth history (Albarède, 2008). Class and Goldstein (2005) pointed out that ocean islands having higher $^3He/^4He$ have depleted (high) time-integrated Sm/Nd, and show elevated $^{143}Nd/^{144}Nd$ compared to expected bulk silicate Earth, suggesting an association between source depletion by partial melting and elevated $^3He/^4He$. Albarède (1998) and Coltice and Ricard (1999) even suggested that bulk solid/melt distribution coefficients for He and U were ~0.01 and ~0.005, respectively, so that mantle residues of partial melting would have lower $U/^3He$ ratios, and over time would tend to show elevated $^3He/^4He$ compared to less depleted mantle regions. They proposed that accumulations of recycled oceanic lithosphere could be the source of high $^3He/^4He$ ratios in basalts derived from deep hotspot sources. According to this model, the accumulated layer of former oceanic lithosphere could have $^3He/^4He$ that was "frozen" at an ancient, high value when the rocks became residual oceanic lithosphere because partial melting stripped it of nearly all its U and Th. Another variation of this model was proposed by Albarède (2008) in which refractory mantle residues such as dunite are recycled into the source region of OIBs, leading to high $^3He/^4He$ because this material was enriched in ancient helium (having elevated $^3He/^4He$) by diffusion, and it is more resistant than fertile lherzolite to the stretching and folding that occurs during mantle convection.

High $^3He/^4He$ values could also result from the incorporation of outer core material into plumes (Porcelli and Halliday, 2001; Bouhifd et al., 2013; Moreira, 2013). Estimates would require this core material to comprise ~0.8 to 3.0% (with very large uncertainties) of the mass of upwelling mantle plumes. Moreira (2013) discussed possible scenarios, using an estimated metal/silicate partition coefficient of 3×10^{-4} from Matsuda et al. (1993), and concluded that the initial mantle [He] would need to have been $>10^6$ times larger than the present day upper mantle concentration if ~1% of core material is present in a mantle plume. This initial [He] is far higher than the highest values observed in chondritic meteorites, which are about 1000 times lower. Bouhifd et al. (2013) measured metal/silicate partition coefficients of 5×10^{-3} to 2×10^{-2}, with no significant pressure effects beyond 6 GPa up to 16 GPa. By assuming that Earth reached its present mass before the solar nebula was dissipated so that gravitationally captured atmospheric gas of solar composition was dissolved into the primordial mantle, they showed that the core could be a viable source of ^3He in mantle plumes throughout geologic time. A correlation between the highest $^3He/^4He$ and highest $^{186}Os/^{188}Os$ in Hawaii was originally used as evidence for a core contribution to both He and Os (Walker et al., 1995). Subsequent studies of Os isotope compositions in other ocean island basalts having elevated $^3He/^4He$, such as Iceland picrites (Brandon et al., 2007), did not show this relation. Studies of the siderophile elements Pt–Re–Os have made it difficult to uniquely tie ocean island basalt chemistry to involvement of the core (e.g., Luguet et al., 2008), and Arevalo and McDonough (2008) showed that entrainment of up to 1 wt.% outer core material would not be detected unambiguously in basalts derived from enriched mantle sources. Possible decoupling in the core–mantle transfer of siderophile elements vs. helium (Dale et al., 2009) or enhanced diffusivity of helium into the core–mantle boundary layer (Moreira, 2013) are additional complications. An accurate assessment of core involvement will eventually require a much better understanding of the partitioning behavior of Pt–Re–Os–W and He at core pressure and in appropriate Fe alloys containing light elements such as Si, C, S and O. For all these reasons, we cannot exclude the core as a potential high $^3He/^4He$ reservoir in the Earth, although we consider the idea to be speculative. We do note that Porcelli and Elliott (2008), taking account of the history of continental crustal growth, showed that high $^3He/^4He$ ratios in ocean island basalts can be plausibly explained by very ancient isolation of part(s) of the Earth's mantle from its dominantly convecting regions.

The results of our study indicate that helium is effectively the most incompatible element during partial melting of mantle peridotite. The presence of high $^3He/^4He$ at many ocean islands and large igneous provinces therefore seems to require significant concentrations of ^3He in their mantle source regions. This would be most plausibly explained by isolation of those sources from convecting mantle regions, and this is more read-

ily achieved at depths near the core–mantle boundary (CMB). The large low shear wave velocity provinces (LLSVPs) and ultra-low velocity zones (ULVZs) above the CMB have captured the imagination of mantle geodynamicists and geochemists (Garnero et al., 2016; White, 2015) and been suggested to be potential reservoirs for Earth's oldest (>4.45 Ga) and least differentiated (primordial?) material. The presence of this ancient material in the deep Earth is established on the basis of the Xe and W isotope differences between hotspot/flood basalt provinces and upper mantle-derived basalts (Mukhopadhyay, 2012; Rizo et al., 2016). The simplest explanation for elevated ^{3}He/^{4}He ratios associated with these ancient Xe and W isotope anomalies is, therefore, that they track material ultimately derived from mantle reservoirs, isolated prior to 4.45 Ga, that have experienced no melt extraction since that time.

The isotopic systematics (Pb–Nd–Sr) of high ^{3}He/^{4}He hotspots have long been taken to indicate complex mantle source histories that do not support the presence of an ancient unmelted mantle reservoir containing primitive noble gas signatures without the additional involvement of both depleted mantle and recycled crustal materials. It has also been established from radiogenic and noble gas isotope systematics in basalts (White, 2015) and from high-resolution simulations of mantle convection (Li et al., 2014) that plumes generated in the deep Earth entrain a variety of materials. These include primordial material arising from thermochemical piles at the base of the mantle (possibly LLSVPs), plus subducted crust and lithosphere that has penetrated into those piles as well as been dispersed/accumulated at shallower mantle depths (Li et al., 2014). In some cases relatively high ^{3}He/^{4}He of 20–30 R_A might therefore result from entrainment of primitive material with recycled, processed material (e.g., Gonnermann and Mukhopadhyay, 2009). Recent work involving Xe isotopes also indicates that a large fraction of the xenon at ocean island hotspots has a recycled origin (Mukhopadhyay, 2012; Peto et al., 2013; Parai and Mukhopadhyay, 2015).

Lastly, because elevated ^{3}He/^{4}He is associated with Ne isotope signatures that have a strong solar-like component (Moreira, 2013), and with ^{129}Xe isotope anomalies generated while ^{129}I was still present during the first 100 Myr of Earth's accretion (Mukhopadhyay, 2012), He–Ne–Xe have not been separated in their geochemical behavior, nor in their ability to trace the >4.45 Ga material. This further attests to the absence of melting in that deep mantle source region since it was last isolated.

A more complicated explanation for the existence of high ^{3}He/^{4}He domains is that helium was redistributed by deep mantle melts, leading to some ^{3}He/(U + Th) enrichment. There currently is no compelling evidence that this is how high ^{3}He/^{4}He source regions originated, although the CMB region is a complex region containing compositional and thermal heterogeneity plus isolated melt pockets (Garnero et al., 2016). It was recently proposed that primordial metallic melt deep in the Earth may be a reservoir for primitive noble gas signatures (Zhang et al., 2016). Small amounts of dense Fe–Ni–S liquids might have been trapped in the mantle following crystallization of an early magma ocean. An alternative is that a primitive Fe-rich silicate melt layer, crystallized from a basal magma ocean near the CMB, hosts the missing budget of K, U and Th that is apparent from the non-complementary balance of continental crust and depleted mantle (Labrosse et al., 2007). Based on current understanding such a putative reservoir has remained geochemically hidden. Nevertheless, if solid–melt partition coefficients in this case are of order 0.01, then dense crystal cumulates of a basal magma ocean (parts of LLSVPs?) might contain primitive noble gas signatures (Coltice et al., 2011). A different model involves crystallization of Fe-rich peridotitic melts within a density trap at depths between ~300–400 km, eventually sinking to the CMB region (Lee et al., 2010). Given the extreme solid/melt effective incompatibility of He inferred from our results, this may have allowed ancient high ^{3}He/^{4}He to become "frozen" into non-primordial (differentiated) Fe-rich material near the CMB. However, Lee et al. (2010) proposed that this process occurred over an extended time period of ~10^9 yr after the Hadean, and so it cannot account for the very ancient Xe and W isotope signatures associated with high ^{3}He/^{4}He in mantle plume source regions.

Remaining uncertainties include the effect of pressure on silicate solid/melt partitioning of helium, and whether or not the silicate solid/melt distribution coefficient for He is ever higher than values for U and Th (e.g., at high extents of melting when clinopyroxene melts out; Jackson et al., 2013). Our helium and trace element results indicate a MORB mantle source that has been more depleted than other depleted MORB sources due to prior loss of a small amount (~1%) of melt. In contrast, the large extents of melting associated with a possible crossover in the solid/melt distribution coefficient for He relative to U and Th (Jackson et al., 2013) would leave vanishingly small amounts of helium in the residue. These residues could never account for the elevated ^{3}He/^{4}He at ocean islands.

In summary, given the observed extreme incompatibility of helium during mantle melting, the presence of a high ^{3}He/^{4}He region in the deep mantle is most plausibly explained by a high ^{3}He/(U + Th) source that experienced no melt removal for time scales close to the age of the Earth.

5. Conclusions

Based on the ratios of helium to incompatible elements in undegassed MORBs, helium behaves as the most incompatible element during mantle melting. Such incompatible behavior could be fully governed by bulk distribution coefficients during melting that are consistent with experimentally determined partition coefficients for olivine, clinopyroxene, orthopyroxene and spinel and mineral abundances in mantle peridotite (Heber et al., 2007; Jackson et al., 2013). The extreme incompatible behavior could also be explained by solid diffusion rates that are much faster for He than for U, Th and REE.

The extremely incompatible behavior of helium during melting of peridotite means that elevated ^{3}He/^{4}He at mantle hotspots such as Hawaii and Iceland do not originate from peridotitic residues of melt depletion. This conclusion is valid whether the extreme incompatibility of helium arises from mineral–melt partitioning (Model A) or from greater helium mobility in the solid mantle (Model B). Elevated ^{3}He/^{4}He ratios at ocean islands and continental hotspots are best explained by mantle plumes sourced deeper in the Earth than the upper mantle source for MORBs. These hotspot source regions are also marked by less depletion in incompatible trace elements than the mantle source for MORBs. Consequently, these deep mantle sources must have a lower (U+Th)/^{3}He ratio than the MORB mantle because they have higher ^{3}He concentrations, and they have therefore experienced less melting/degassing over Earth's history. This conclusion is consistent with collective evidence based on all the noble gases (e.g., Marty, 2012; Mukhopadhyay, 2012; Moreira, 2013). Deep mantle sources having high ^{3}He/^{4}He were formed very early in Earth history and have remained isolated since 4.45 Ga.

Acknowledgements

This study was supported by NSF grants OCE 12-59964 and 15-58798 to DG and OCE 12-59916 and 15-58802 to PM. Adam Kent helped guide the laser ablation analyses. We thank Ken Rubin, John Lupton and Marc Hirschmann for helpful discussions. We also thank Sujoy Mukhopadhyay and two anonymous reviewers for constructive comments, and Bernard Marty for editorial handling.

The basalt glasses were collected on a large number of seagoing expeditions involving the authors and other investigators. We thank the Smithsonian, URI and OSU rock repositories for providing sample material, and Mike Perfit for splits of glass from sample ALV2384.

Appendix A. Supplementary material

Supplementary material related to this article can be found online at http://dx.doi.org/10.1016/j.epsl.2016.09.016.

References

Albarède, F., 1998. Time-dependent models of U–Th–He and K–Ar evolution and the layering of mantle convection. Chem. Geol. 145, 413–429.

Albarède, F., 2008. Rogue mantle helium and neon. Science 319, 943–945.

Allègre, C.J., Treuil, M., Minster, J.-F., Minster, B., Albarède, F., 1977. Systematic use of trace elements in igneous processes. Contrib. Mineral. Petrol. 60, 57–75.

Anderson, D.L., 1998. The helium paradoxes. Proc. Natl. Acad. Sci. 95, 4822–4827.

Arevalo, R., McDonough, W.F., 2008. Tungsten geochemistry and implications for understanding the Earth's interior. Earth Planet. Sci. Lett. 272, 656–665.

Beattie, P., 1993a. The generation of uranium series disequilibria by partial melting of spinel peridotite: constraints from partitioning studies. Earth Planet. Sci. Lett. 117, 379–391.

Beattie, P., 1993b. Uranium–thorium disequilibria and partitioning on melting of garnet peridotite. Nature 363, 63–65.

Blundy, J., Wood, B.J., 2003. Partitioning of trace elements between crystals and melts. Earth Planet. Sci. Lett. 210, 383–397.

Bougault, H., Dmitriev, L., Schilling, J.-G., Sobolev, A., Joron, J.L., Needham, H.D., 1988. Mantle heterogeneity from trace elements: MAR triple junction near 14°N. Earth Planet. Sci. Lett. 88, 27–36.

Bouhifd, M.A., Jephcoat, A.P., Heber, V.S., Kelley, S.P., 2013. Helium in Earth's early core. Nat. Geosci. 6, 982–986.

Brandon, A.D., Graham, D.W., Waight, T., Gautason, B., 2007. ^{186}Os and ^{187}Os enrichments and high-^{3}He/^{4}He sources in the Earth's mantle: evidence from Icelandic picrites. Geochim. Cosmochim. Acta 71, 4570–4591.

Brooker, R.A., Du, Z., Blundy, J.D., Kelley, S.P., Allan, N.J., Wood, B.J., Chamorro, E., Wartho, J.-A., Purton, J.A., 2003. The 'zero charge' partitioning behaviour of noble gases during mantle melting. Nature 423, 738–741.

Burnard, P., 2004. Diffusive fractionation of noble gases and helium isotopes during mantle melting. Earth Planet. Sci. Lett. 220, 287–295.

Burnard, P.G., Demouchy, S., Delon, R., Arnaud, N.O., Marrocchi, Y., Cordier, P., Addad, A., 2015. The role of grain boundaries in the storage and transport of noble gases in the mantle. Earth Planet. Sci. Lett. 430, 260–270.

Cartigny, P., Pineau, F., Aubaud, C., Javoy, M., 2008. Towards a consistent mantle carbon flux estimate: insights from volatile systematics (H_2O/Ce, ∂D, CO_2/Nb) in the North Atlantic mantle. Earth Planet. Sci. Lett. 265, 672–685.

Cherniak, D.J., Dimanov, A., 2010. Diffusion in pyroxene, mica and amphibole. In: Zhang, Y., Cherniak, D.J. (Eds.), Rev. Mineral. Geochem. 72, Mineral. Soc. Amer., 641–690.

Class, C., Goldstein, S.L., 2005. Evolution of helium isotopes in the Earth's mantle. Nature 436, 1107–1112.

Coltice, N., Ricard, Y., 1999. Geochemical observations and one layer mantle convection. Earth Planet. Sci. Lett. 174, 125–137.

Coltice, N., Moreira, M., Hernlund, J., Labrosse, S., 2011. Crystallization of a basal magma ocean recorded by helium and neon. Earth Planet. Sci. Lett. 308, 193–199.

Dale, C.W., Pearson, D.G., Starkey, N.A., Stuart, F.M., Ellam, R.M., Larsen, L.M., Fitton, J.G., Macpherson, C.G., 2009. Osmium isotopes in Baffin Island and West Greenland picrites: implications for the ^{187}Os/^{188}Os composition of the convecting mantle and the nature of high ^{3}He/^{4}He mantle. Earth Planet. Sci. Lett. 278, 267–277.

Dasgupta, R., Hirschmann, M.M., 2006. Melting in the Earth's deep upper mantle caused by carbon dioxide. Nature 440, 659–662.

Davies, G.F., 2010. Noble gases in the dynamic mantle. Geochem. Geophys. Geosyst. 11, 1–17.

Dixon, J.E., Clague, D.A., Wallace, P., Poreda, R., 1997. Volatiles in alkalic basalts from the North Arch volcanic field, Hawaii: extensive degassing of deep submarine-erupted alkalic series lavas. J. Petrol. 38, 911–939.

Garnero, E.J., McNamara, A.K., Shim, S.-H., 2016. Continent-sized anomalous zones with low seismic velocity at the base of Earth's mantle. Nat. Geosci. 9, 481–489.

Gast, P.W., 1968. Trace element fractionation and the origin of tholeiitic and alkaline magma types. Geochim. Cosmochim. Acta 32, 1057–1086.

Gautheron, C., Moreira, M., Gerin, C., Tassan-Got, L., Bezos, A., Humler, E., 2015. Constraints on the DUPAL anomaly from helium isotope systematics in the Southwest Indian mid-ocean ridge basalts. Chem. Geol. 417, 163–172.

Goldstein, S.L., Soffer, G., Langmuir, C.H., Lehnert, K.A., Graham, D.W., Michael, P.J., 2008. Origin of a 'southern hemisphere' geochemical signature in the Arctic upper mantle. Nature 453, 89–94.

Gonnermann, H., Mukhopadhyay, S., 2009. Preserving noble gases in a convecting mantle. Nature 459, 560–564.

Graham, D.W., Jenkins, W.J., Schilling, J.-G., Thompson, G., Kurz, M.D., Humphris, S.E., 1992. Helium isotope geochemistry of mid-ocean ridge basalts from the South Atlantic. Earth Planet. Sci. Lett. 110, 133–147.

Graham, D.W., Lupton, J.E., Spera, F.J., Christie, D.M., 2001. Upper mantle dynamics revealed by helium isotope variations along the Southeast Indian Ridge. Nature 409, 701–703.

Graham, D.W., Hanan, B.B., Hémond, C., Blichert-Toft, J., Albarède, F., 2014. Helium isotopic textures in Earth's upper mantle. Geochem. Geophys. Geosyst. 15, 2048–2074.

Gregg, P.M., Behn, M.D., Lin, J., Grove, T.L., 2009. Melt generation, crystallization, and extraction beneath segmented oceanic transform faults. J. Geophys. Res. 114.

Hamelin, C., Dosso, L., Hanan, B.B., Moreira, M., Kositsky, A.P., Thomas, M.Y., 2011. Geochemical portray of the Pacific Ridge: new isotopic data and statistical techniques. Earth Planet. Sci. Lett. 302, 154–162.

Hart, S.R., 1993. Equilibration during mantle melting: a fractal tree model. Proc. Natl. Acad. Sci. USA 90, 11914–11918.

Hart, S.R., Kurz, M., Wang, Z., 2008. Scale length of mantle heterogeneities: constraints from helium diffusion. Earth Planet. Sci. Lett. 269, 507–516.

Hartley, M.E., Maclennan, J., Edmonds, M., Thordarson, T., 2014. Reconstructing the deep CO_2 degassing behaviour of large basaltic fissure eruptions. Earth Planet. Sci. Lett. 393, 120–131.

Hayden, L.A., Watson, E.B., 2008. Grain boundary mobility of carbon in Earth's mantle: a possible carbon flux from the core. Proc. Natl. Acad. Sci. 105, 8537–8541.

Heber, V.S., Brooker, R.A., Kelley, S.P., Wood, B.J., 2007. Crystal–melt partitioning of noble gases (helium, neon, argon, krypton, and xenon) for olivine and clinopyroxene. Geochim. Cosmochim. Acta 71, 1041–1061.

Helo, C., Longpré, M.A., Shimizu, N., Clague, D.A., Stix, J., 2011. Explosive eruptions at mid-ocean ridges driven by CO_2-rich magmas. Nat. Geosci. 4, 260–263.

Hirano, N., Takahashi, E., Yamamoto, J., Abe, N., Ingle, S.P., Kaneoka, I., Hirata, T., Kimura, J.-i., Ishii, T., Ogawa, Y., Machida, S., Suyehiro, K., 2006. Volcanism in response to plate flexure. Science 313, 1426–1428.

Hirschmann, M.M., Dasgupta, R., 2009. The H/C ratios of Earth's near-surface and deep reservoirs, and consequences for deep Earth volatile cycles. Chem. Geol. 262, 4–16.

Hiyagon, H., Ozima, M., 1986. Partition of noble gases between olivine and basalt melt. Geochim. Cosmochim. Acta 50, 2045–2057.

Jackson, C.R.M., Parman, S.W., Kelley, S.P., Cooper, R.F., 2013. Constraints on light noble partitioning at the conditions of spinel-peridotite melting. Earth Planet. Sci. Lett. 384, 178–187.

Keller, T., Katz, R.F., Hirschmann, M.M., in press. The fate of volatiles in mid-ocean ridge magmatism. Earth Planet. Sci. Lett. arXiv:1608.03841v1.

Kelley, K.A., Kingsley, R., Schilling, J.-G., 2013. Composition of plume-influenced mid-ocean ridge lavas and glasses from the Mid-Atlantic Ridge, East Pacific Rise, Galápagos Spreading Center, and Gulf of Aden. Geochem. Geophys. Geosyst. 14, 223–242.

Kurz, M.D., 1993. Mantle heterogeneity beneath oceanic islands: some inferences from isotopes. Philos. Trans. R. Soc. Lond. A 342, 91–103.

Kurz, M.D., Jenkins, W.J., Hart, S.R., 1982. Helium isotopic systematics of oceanic islands and mantle heterogeneity. Nature 297, 43–46.

Kurz, M.D., Moreira, M., Curtice, J., Lott, D.E., Mahoney, J.J., Sinton, J.M., 2005. Correlated helium, neon, and melt production on the super-fast spreading East Pacific Rise near 17°S. Earth Planet. Sci. Lett. 232, 125–142.

Labrosse, S., Hernlund, J., Coltice, N., 2007. A crystallizing dense magma ocean at the base of the Earth's mantle. Nature 450, 866–870.

LaTourrette, T.Z., Burnett, D.S., 1992. Experimental determination of U and Th partitioning between clinopyroxene and natural and synthetic basaltic liquid. Earth Planet. Sci. Lett. 110, 227–244.

LaTourrette, T.Z., Kennedy, A.K., Wasserburg, G.J., 1993. Thorium–uranium fractionation by garnet: evidence for a deep source and rapid rise of oceanic basalts. Science 261, 739–742.

Lee, C.-T., Luffi, P., Höink, T., Li, J., Dasgupta, R., Hernlund, J., 2010. Upside-down differentiation and generation of 'primordial' mantle. Nature 463, 930–935.

Li, M., McNamara, A.K., Garnero, E.J., 2014. Chemical complexity of hotspots caused by cycling oceanic crust through mantle reservoirs. Nat. Geosci. 7, 366–370.

Luguet, A., Pearson, D.G., Nowell, G.M., Dreher, S.T., Coggon, J.A., Spetsius, Z.V., Parman, S.W., 2008. Enriched Pt–Re–Os isotope systematics in plume lavas explained by metasomatic sulfides. Science 319, 453–456.

Lupton, J.E., Graham, D.W., Delaney, J.R., Johnson, H.P., 1993. Helium isotope variations in Juan de Fuca Ridge basalts. Geophys. Res. Lett. 20, 1851–1854.

Marty, B., 2012. The origins and concentrations of water, carbon, nitrogen and noble gases on Earth. Earth Planet. Sci. Lett. 313–314, 56–66.

Marty, B., Jambon, A., 1987. C/^{3}He in volatile fluxes from the solid Earth: implications for carbon geodynamics. Earth Planet. Sci. Lett. 83, 16–26.

Marty, B., Lussiez, P., 1993. Constraints on rare gas partition coefficients from analysis of olivine-glass from a picritic mid-ocean ridge basalt. Chem. Geol. 106, 1–7.

Marty, B., Zimmerman, L., 1999. Volatiles (He, C, N, Ar) in mid-ocean ridge basalts: assessment of shallow-level fractionation and characterization of source composition. Geochim. Cosmochim. Acta 63, 3619–3633.

Matsuda, J., Sudo, M., Ito, K., Oktaka, O., Ito, E., 1993. Noble gas partitioning between metal and silicate under high pressures. Science 259, 788–790.
McDade, P., Blundy, J.D., Wood, B.J., 2003. Trace element partitioning on the Tinaquillo lherzolite solidus at 1.5 GPa. Phys. Earth Planet. Inter. 139, 129–147.
Michael, P.J., Graham, D.W., 2015. The behavior and concentration of CO_2 in the suboceanic mantle: inferences from undegassed ocean ridge and ocean island basalts. Lithos 236–237, 338–351.
Michael, P.J., Langmuir, C.H., Dick, H.J.B., Snow, J.E., Goldstein, S.L., Graham, D.W., Lehnert, K., Kurras, G., Jokat, W., Mühe, R., Edmonds, H.N., 2003. Magmatic and amagmatic seafloor generation at the ultraslow-spreading Gakkel Ridge, Arctic Ocean. Nature 423, 956–961.
Moreira, M., 2013. Noble gas constraints on the origin and evolution of Earth's volatiles. Geochem. Perspect. 2, 229–403.
Mukhopadhyay, S., 2012. Early differentiation and volatile accretion recorded in deep-mantle neon and xenon. Nature 486, 101–104.
Navon, O., Stolper, E., 1987. Geochemical consequences of melt percolation: the upper mantle as a chromatographic column. J. Geol. 95, 285–307.
Newman, S., Lowenstern, J.B., 2002. VolatileCalc: a silicate melt–H_2O–CO_2 solution model written in Visual Basic for Excel. Comput. Geosci. 28, 597–604.
Parai, R., Mukhopadhyay, S., 2015. The evolution of MORB and plume mantle volatile budgets: constraints from fission Xe isotopes in Southwest Indian Ridge basalts. Geochem. Geophys. Geosyst. http://dx.doi.org/10.1002/2014GC005566.
Parman, S.W., Kurz, M.D., Hart, S.R., Grove, T.L., 2005. Helium solubility in olivine and implications for high $^3He/^4He$ in ocean island basalts. Nature 437, 1140–1143.
Peto, M.K., Mukhopadhyay, S., Kelley, K.A., 2013. Heterogeneities from the first 100 million years recorded in deep mantle noble gases from the Northern Lau Back-arc Basin. Earth Planet. Sci. Lett. 369–370, 13–23.
Pilet, S., Baker, M.B., Müntener, O., Stolper, E.M., 2011. Monte Carlo simulations of metasomatic enrichment in the lithosphere and implications for the source of alkaline basalts. J. Petrol. 52, 1415–1442.
Porcelli, D., Elliott, T., 2008. The evolution of helium isotopes in the upper mantle and the generation of isotopic anomalies. Earth Planet. Sci. Lett. 269, 175–185.
Porcelli, D., Halliday, A.N., 2001. The core as a possible source of mantle helium. Earth Planet. Sci. Lett. 192, 45–56.
Qin, Z., 1992. Disequilibrium partial melting model and its implications for trace element fractionations during mantle melting. Earth Planet. Sci. Lett. 112, 75–90.
Rizo, H., Walker, R.J., Carlson, R.W., Horan, M.F., Mukhopadhyay, S., Manthos, V., Francis, D., Jackson, M.G., 2016. Preservation of Earth-forming events in the tungsten isotopic composition of modern flood basalts. Science 352, 809–812.
Salters, V.J.M., Stracke, A., 2004. Composition of the depleted mantle. Geochem. Geophys. Geosyst. 5. Paper 2003GC000597.
Shcheka, S.S., Wiedenbeck, M., Frost, D.J., Keppler, H., 2006. Carbon solubility in mantle minerals. Earth Planet. Sci. Lett. 245, 730–742.
Shilobreeva, S.N., Kuzmin, L.E., Kazantsev, A.M., 2000. Nuclear reaction and SIMS studies of carbon diffusion in olivines. Nucl. Instrum. Methods Phys. Res., Sect. B, Beam Interact. Mater. Atoms 161–163, 797–800.
Spiegelman, M., Kenyon, P., 1992. The requirements for chemical disequilibrium during magma migration. Earth Planet. Sci. Lett. 109, 611–620.
Stagno, V., Ojwang, D., McCammon, C.A., Frost, D.J., 2013. The oxidation state of the mantle and the extraction of carbon from Earth's interior. Nature 493, 84–90.
Stroncik, N., Niedermann, S., 2016. He, Ne and Ar isotope signatures of mid-ocean ridge basalts and their implications for upper mantle structure: a case study from the Mid-Atlantic Ridge at 4–12°S. Geochim. Cosmochim. Acta 183, 94–105.
Sun, S.-S., McDonough, W.F., 1989. Chemical and isotopic systematics of oceanic basalts: implications for mantle composition and processes. In: Saunders, A.D., Norry, M.J. (Eds.), Magmatism in the Ocean Basins. Geol. Soc. Lond., pp. 313–345.
Trull, T.W., Kurz, M.D., 1993. Experimental measurements of ^3He and ^4He mobility in olivine and clinopyroxene at magmatic temperatures. Geochim. Cosmochim. Acta 57, 1313–1324.
Tucker, J.M., Mukhopadhyay, S., Schilling, J.-G., 2012. The heavy noble gas composition of the depleted MORB mantle (DMM) and its implications for the preservation of heterogeneities in the mantle. Earth Planet. Sci. Lett. 355–356, 244–254.
Van Orman, J.A., Grove, T.L., Shimizu, N., 2002. Diffusive fractionation of trace elements during production and transport of melt in Earth's upper mantle. Earth Planet. Sci. Lett. 198, 93–112.
Walker, R.J., Morgan, J.W., Horan, M.F., 1995. Osmium-187 enrichment in some plumes: evidence for core–mantle interaction? Science 269, 819–822.
Wanless, V.D., Shaw, A.M., 2012. Lower crustal crystallization and melt evolution at mid-ocean ridges. Nat. Geosci. 5, 651–655.
White, W.M., 2015. Isotopes, DUPAL, LLSVPs, and Anekantavada. Chem. Geol. 419, 10–28.
Workman, R.K., Hart, S.R., 2005. Major and trace element composition of the depleted MORB mantle (DMM). Earth Planet. Sci. Lett. 231, 53–72.
Zhang, Z., Dorfman, S.M., Labidi, J., Zhang, S., Li, M., Manga, M., Stixrude, L., McDonough, W.F., Williams, Q., 2016. Primordial metallic melt in the deep mantle. Geophys. Res. Lett. 43, 3693–3699.